Comparative Biochemistry and Physiology, Part C 183–184 (2016) 36–45

Contents lists available at ScienceDirect

Comparative Biochemistry and Physiology, Part C

journal homepage: www.elsevier.com/locate/cbpc

Computational model of the fathead minnow hypothalamic–pituitary–gonadal axis: Incorporating protein synthesis in improving predictability of responses to endocrine active chemicals

Miyuki Breen [a], Daniel L. Villeneuve [b], Gerald T. Ankley [b], David Bencic [c], Michael S. Breen [d], Karen H. Watanabe [e], Alun L. Lloyd [a], Rory B. Conolly [f,*]

[a] Biomathematics Graduate Program, Department of Mathematics, North Carolina State University, Box 8203, Raleigh, NC 27695, USA
[b] Mid-Continent Ecology Division, National Health and Environmental Effects Research Laboratory, U.S. Environmental Protection Agency, 6201 Congdon Blvd, Duluth, MN 55804, USA
[c] Ecological Exposure Research Division, National Exposure Research Laboratory, U.S. Environmental Protection Agency, Cincinnati, OH, USA
[d] National Exposure Research Laboratory, U.S. Environmental Protection Agency, 109 TW Alexander Drive, Research Triangle Park, NC 27711, USA
[e] Division of Environmental and Biomolecular Systems, Institute of Environmental Health, Oregon Health & Science University, 3181 SW Sam Jackson Park Road HRC3, Portland, OR 97239, USA
[f] Integrated Systems Toxicology Division, National Health and Environmental Effects Research Laboratory, U.S. Environmental Protection Agency, 109 TW Alexander Drive, Research Triangle Park, NC 27711, USA

ARTICLE INFO

Article history:
Received 30 October 2015
Received in revised form 8 February 2016
Accepted 9 February 2016
Available online 12 February 2016

Keywords:
Adaptation
Computational model
Endocrine disrupting chemicals
Fadrozole
Fish
Hypothalamic–pituitary–gonadal axis
Protein synthesis
Toxicology

ABSTRACT

There is international concern about chemicals that alter endocrine system function in humans and/or wildlife and subsequently cause adverse effects. We previously developed a mechanistic computational model of the hypothalamic–pituitary–gonadal (HPG) axis in female fathead minnows exposed to a model aromatase inhibitor, fadrozole (FAD), to predict dose–response and time-course behaviors for apical reproductive endpoints. Initial efforts to develop a computational model describing adaptive responses to endocrine stress providing good fits to empirical plasma 17β-estradiol (E2) data in exposed fish were only partially successful, which suggests that additional regulatory biology processes need to be considered. In this study, we addressed short-comings of the previous model by incorporating additional details concerning CYP19A (aromatase) protein synthesis. Predictions based on the revised model were evaluated using plasma E2 concentrations and ovarian cytochrome P450 (CYP) 19 A aromatase mRNA data from two fathead minnow time-course experiments with FAD, as well as from a third 4-day study. The extended model provides better fits to measured E2 time-course concentrations, and the model accurately predicts *CYP19A* mRNA fold changes and plasma E2 dose–response from the 4-d concentration–response study. This study suggests that aromatase protein synthesis is an important process in the biological system to model the effects of FAD exposure.

1. Introduction

There is international concern about environmental contaminants, commercial products and drugs that alter endocrine system function in humans and/or wildlife and subsequently cause adverse effects (Cooper and Kavlock, 1997; Daston et al., 2003; Hutchinson et al., 2006; Zacharewski, 1998). The Safe Drinking Water Act Amendments (1996) and the Food Quality Protection Act (1996) require the U.S. Environmental Protection Agency (EPA) to screen for endocrine-active chemicals in drinking water and pesticides used in food production. Based on this legislation, the EPA developed and implemented a multi-phased screening (Tier 1) and testing (Tier 2) process called the Endocrine Disruptor Screening Program (EDSP; U.S. Environmental Protection Agency,, 1998, 2009). Steroid biosynthesis inhibitors, including aromatase inhibitors, were recognized as an important class of endocrine disruptors and were selected for evaluation in the EDSP (Drenth et al., 1998; Sanderson, 2006; Vinggaard et al., 2000; U.S. Environmental Protection Agency, 1998). One of the functions of EDSP Tier 2 is to characterize the dose–response of chemicals that can interact with the endocrine system, reflecting the importance of understanding the dose–response behavior of endocrine disruptors.

The dose–response and time-course (DRTC) behavior of organisms exposed to environmental chemicals are major determinants of health risk. In addition to factors like adsorption, distribution, metabolism, and elimination, physiological adaptation or compensation can be a major determinant of the occurrence of adverse effects. Understanding

* Corresponding author at: U.S. Environmental Protection Agency, Office of Research and Development, National Health and Environmental Effects Research Laboratory, 109 T.W. Alexander Drive, Mail B105-03, Research Triangle Park, NC 27711, USA. Tel.: +1 919 541 9782.
E-mail addresses: mbreen@ncsu.edu (M. Breen), villeneuve.dan@epa.gov (D.L. Villeneuve), ankley.gerald@epa.gov (G.T. Ankley), bencic.david@epa.gov (D. Bencic), breen.michael@epa.gov (M.S. Breen), watanabk@ohsu.edu (K.H. Watanabe), alun_lloyd@ncsu.edu (A.L. Lloyd), conolly.rory@epa.gov (R.B. Conolly).

http://dx.doi.org/10.1016/j.cbpc.2016.02.002
1532-0456/

compensatory responses is critical to the modern practice of toxicology, particularly as the field evolves from traditional reliance on whole animal testing with apical endpoints toward more predictive approaches anchored to an understanding of chemical modes of action. In recognition of this, the U.S. National Research Council report, *Toxicity Testing in the 21st Century*: *A Vision and a Strategy*, emphasizes that adaptive changes within organisms exposed to environmental stress can alter dose–response behaviors to modulate stressor effects (National Research Council, 2007). Consequently, to improve descriptions of dose–response behaviors for risk assessment, a better understanding of adaptive mechanisms is needed. Hence, a goal of our larger research effort (Ankley et al., 2009) has been to develop a computational model of adaptive mechanisms in the hypothalamic–pituitary–gonadal (HPG) axis for a model vertebrate, the fathead minnow (*Pimephales promelas*).

In initial studies, we developed a mathematical model to predict the DRTC behaviors in the HPG axis of female fathead minnows exposed to model aromatase inhibitor, fadrozole (FAD; Breen et al., 2013). Fadrozole competitively inhibits the steroidogenic enzyme aromatase, a cytochrome P450 (CYP) 19 A, which is rate-limiting in the conversion of testosterone (T) to 17β-estradiol (E2) (Miller, 1988). While FAD itself is not ecologically relevant, there are a variety of environmental contaminants that can inhibit aromatase activity and elicit similar effects (Petkov et al., 2009; Vinggaard et al., 2000). The initial deterministic model included a feedback regulatory loop within the HPG axis to

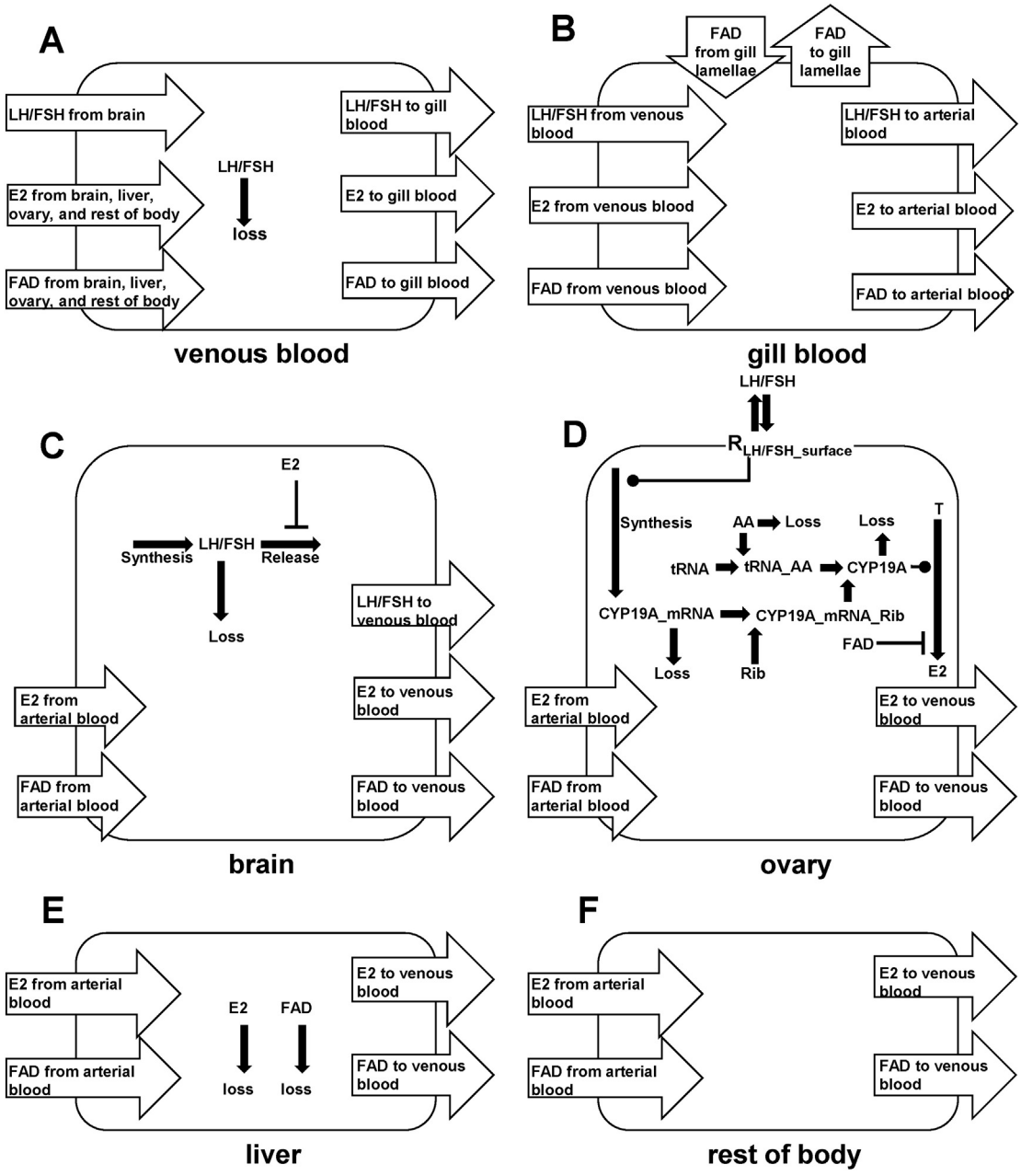

Fig. 1. Graphical representation of biochemical processes within the six compartments of the model: venous blood (A), gill blood (B), brain (C), ovary (D), liver (E), and rest of body (F). In the venous blood (A), processes include: uptake and release of LH/FSH, E2, and FAD; degradation of LH/FSH. In the gill (B), processes include: uptake and release of LH/FSH, E2, and FAD; FAD transport from gill lamellae to gill blood. In the brain (C), processes include: uptake and release of FAD and E2; LH/FSH synthesis, release, and degradation; E2-mediated inhibition of LH/FSH release into venous blood. In the ovary (D), processes include: uptake and release of FAD and E2; reversible binding of LH/FSH in blood to LH/FSH receptors on cell membrane (surface); LH/FSH receptor-mediated activation of CYP19A_mRNA synthesis; binding of CYP19A_mRNA to ribosome (Rib); binding of amino acids (AA) to transfer RNA (tRNA); translation of CYP19A_mRNA into CYP19A by CYP19A_mRNA_Rib complex and tRNA_AA; degradation of AA, CYP19A_mRNA, and CYP19A; conversion of T into E2 catalyzed by CYP19A; enzyme inhibition of CYP19A by FAD. In the liver (E), processes includes: uptake and release of E2 and FAD; degradation of E2 and FAD. In the rest of body (F), processes include uptake and release of FAD and E2.

mediate adaptive responses to endocrine-active chemical stressors by controlling the secretion of luteinizing hormone (LH) and follicle-stimulating hormone (FSH) from a generalized HP complex (Breen et al., 2013). In the present paper, we build upon the previously described model to address a key limitation in its predictive ability to improve the congruence between model predictions and empirical data.

The primary focus of our previous work was on adaptive changes (compensation) in plasma E2 concentrations during FAD exposure, which resulted in a period of increased E2 production/concentration, relative to controls, immediately following removal of the inhibitor (an overshoot), particularly at lower FAD concentrations (Breen et al., 2013). The main limitation of the previous HPG axis model was a large overestimation of plasma E2 concentrations for higher FAD test concentrations. In the present paper, we address this limitation by investigating protein synthesis of CYP19A. Because protein synthesis and degradation are responsible for amounts of CYP19A available for the conversion of T to E2, we extended the previous model by adding the CYP19A protein synthesis pathway.

The contribution of this study is the extension of the previously developed HPG axis model (Breen et al., 2013). The extended model was evaluated with measurements of plasma E2 and ovarian *CYP19A* mRNA for eight FAD test concentrations. Comparing the model-predicted and measured data provides insights into possible feedback control mechanisms embedded in the HPG axis.

2. Materials and methods

2.1. FAD exposure

The model described in the present study incorporates data from three experiments with fathead minnows exposed to FAD. The first of these studies is described in detail by Villeneuve et al. (2009). Briefly, sexually-mature fathead minnows (5–6 month old), obtained from an onsite culture facility at the EPA Mid-Continent Ecology Division (Duluth, MN), were exposed to 0, 3, or 30 μg FAD/L. Fadrozole was delivered to 20 L tanks containing 10 L of test solution via a continuous flow (approximately 45 ml/min) of UV-treated, filtered Lake Superior water without use of a carrier solvent. Four male and four female fathead minnows were exposed in each tank. The experiment was initiated by transferring random groups of fish directly to tanks that had been receiving a continuous flow of test solution for approximately 48 h. Addition of fish was staggered by replicate within each treatment to permit all samples from a given exposure tank to be collected within 45 min of the desired exposure duration. Two tanks of four male and four female fish were sacrificed after 1, 2, 4, and 8 d of exposure. After 8 days of exposure, remaining fish were held in control Lake Superior water (no FAD) and sampled after 1, 2, 4, or 8 d of depuration. There were two replicate tanks for each unique exposure condition (i.e., combination of treatment and time point). Urine, plasma, liver, gonad, brain, and pituitary samples were collected and a variety of endocrine and toxicogenomic endpoints were examined. In total, Villeneuve et al. (2009) reported results for over 15 different endocrine-related variables. However, for the current modeling work, major endpoints of interest were plasma concentrations of E2 and ovarian expression of CYP19A. Notably, CYP19A protein concentrations were not measured.

The second experiment (Villeneuve et al., 2013) was a follow-up to the study described above, only with extended time-course. Briefly, reproductively-mature fathead minnows were exposed to 0, 0.5, or 30 μg FAD/L using conditions similar to those described above. Fish were either exposed continuously and sampled after 1, 8, 12, 16, 20, 24, or 28 d of exposure or exposed for 8 d, then held in a continuous flow of clean Lake Superior water for an additional 4, 8, 12, 16, or 20 d. Various endpoints were analyzed, including plasma E2 and ovarian *CYP19A* mRNA.

In a third experiment (Ralston-Hooper et al., 2013), fathead minnows were exposed to 0, 0.04, 0.2, 1, or 5 μg FAD/L for 4 d under conditions similar to those described above and various endpoints were analyzed, including plasma E2 concentrations.

2.2. Mathematical model of the HPG-axis

The extended computational model of the HPG axis for FAD-exposed female fathead minnow described herein is a modification of our previously-described HPG axis model (Breen et al., 2013). As does the model of Breen et al. (2013), the extended model consists of six tissue compartments: gill, brain, ovary, liver, venous blood, and rest of body (Fig. 1). These compartments, which are involved in HPG axis signaling and feedback control, are connected in a manner consistent with the cardiovascular system of fish. The model includes a generalized regulatory feedback loop within the HPG axis that mediates adaptive responses to endocrine stress from FAD. The regulatory negative feedback loop controls the secretion of gonadotropins (LH and FSH) from the brain, which is regulated by amount of E2 secreted from

Table 1
Estimated parameters.

Parameter description	Symbol	Compartment	Value
Basal synthesis rate of CYP19A mRNA	$k_{syn\_mRNA\_basal}$	Ovary	5.126×10^{-7} μmol-h^{-1}
Maximum synthesis rate of CYP19A mRNA	$k_{syn\_mRNA\_max}$	Ovary	6.797×10^{-1} μmol-h^{-1}
Degradation rate of CYP19A mRNA	k_{loss_mRNA}	Ovary	2.861×10^{-2} h^{-1}
Maximum synthesis rate of CYP19A	$k_{cat\_CYP19A\_mRNA}$	Ovary	5.741×10^{-2} h^{-1}
Michaelis constant for synthesis of CYP19A	$K_{m\_syn\_CYP19A}$	Ovary	6.471×10^{4} μmol-L^{-1}
Degradation rate of CYP19A	k_{loss_CYP19A}	Ovary	3.007×10^{-2} h^{-1}
Inhibition constant of FAD	K_{i_FAD}	Ovary	4.273×10^{-3} μmol-L^{-1}
Activation constant for synthesis CYP19A mRNA	$K_{a\_syn\_mRNA}$	Ovary	6.784×10^{-22} μmol-L^{-1}
Total amount of ribosome	A_{rib_total}	Ovary	9.551×10^{-3} μmol
Binding rate of ribosome with CYP19A mRNA	k_{rib_on}	Ovary	2.041×10^{1} μmol^{-1}-h^{-1}
Releasing rate of ribosome with CYP19A mRNA	k_{rib_off}	Ovary	1.840×10^{-5} h^{-1}
Synthesis rate of AA	k_{syn_AA}	Ovary	1.106×10^{1} μmol-h^{-1}
Degradation rate of AA	k_{loss_AA}	Ovary	2.103 h^{-1}
Binding rate of AA with tRNA	k_{tRNA_on}	Ovary	9.180 μmol^{-1}-h^{-1}
Releasing rate of AA from tRNA	k_{tRNA_off}	Ovary	7.082×10^{-1} h^{-1}
Degradation rate of FAD	k_{loss_FAD}	Liver	5.585×10^{-1} h^{-1}
Degradation rate of E2	k_{loss_E2}	Liver	4.327 h^{-1}
Zero-order synthesis rate of LHFSH	$k_{0\_syn\_LHFSH}$	Brain	5.308×10^{-10} μmol-h^{-1}
Degradation rate of LHFSH	k_{loss_LHFSH}	Brain	1.416×10^{2} h^{-1}
Releasing rate of LHFSH	k_{LHFSH}	Brain	2.503×10^{-3} h^{-1}
Inhibition constant of E2	K_{i_E2}	Brain	4.812×10^{-5} μmol-L^{-1}
Releasing rate of LHFSH (blood) from LHFSH receptor (ovary)	k_{LHFSH_off}	Venous Blood	7.792×10^{-1} h^{-1}
Degradation rate of LHFSH	k_{loss_LHFSH}	Venous Blood	2.795 h^{-1}

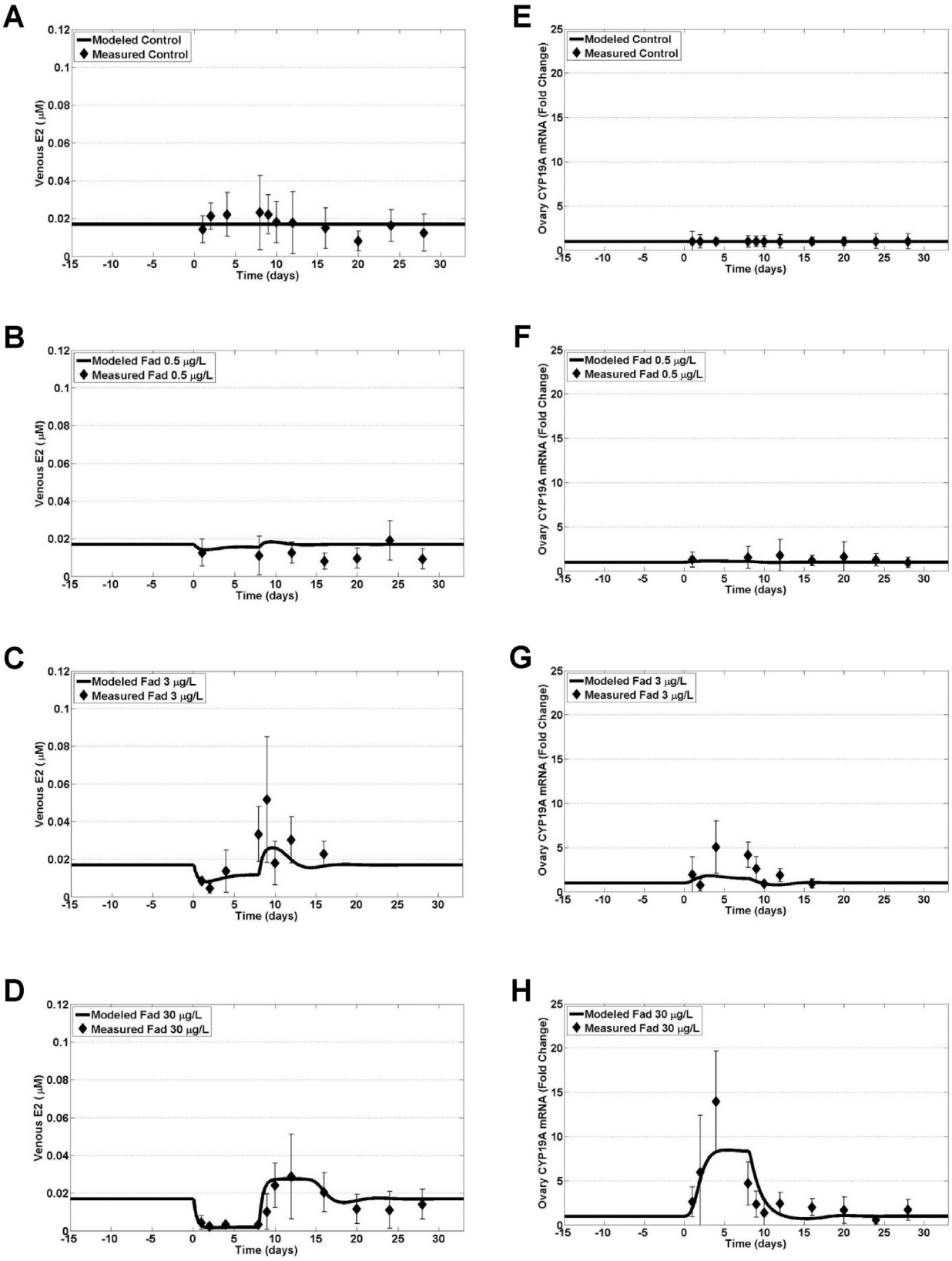

Fig. 2. Model evaluation for control and three FAD concentrations (0.5 μg/L, 3 μg/L, and 30 μg/L). Model-predictions were plotted as a function of days during pre-exposure (−15–0 days), exposure to FAD (0–8 days), and post-exposure (8–33 days), and compared with measurements (mean ± SD) for plasma E2 concentrations (A–D) and ovary CYP19A_mRNA fold changes relative to controls (E–H). Model-predictions were compared with measurement data from two experiments: control data includes four sampling times during exposure and seven sampling times post-exposure; 0.5 μg/L—two sampling times during exposure and five sampling times post-exposure; 3 μg/L—four sampling times during exposure and four sampling times post-exposure; 30 μg/L—four sampling times during exposure and seven sampling times post-exposure.

ovary. The descriptions of each tissue compartment were previously reported by Breen et al. (2013), with the exception of CYP19A protein synthesis in the ovary (Fig. 1D). Protein synthesis involves two major processes: transcription and translation. In the nucleus, transcription occurs when an RNA polymerase enzyme binds to DNA to start the production of messenger RNA (mRNA). The mRNA then leaves the nucleus and enters the cytoplasm to bind to ribosomes. In the cytoplasm, amino acids (AA) bind to transfer RNA (tRNA) and are transported to ribosomes. At the ribosome, translation occurs when a series of tRNA molecules bind to mRNA to form a chain of AA that creates a protein (Bruce et al., 2002; Campbell, 1996). In the extended model, the rate of protein synthesis for CYP19A is a function of levels of mRNA, ribosomes, tRNA, and AA. Once *CYP19A* mRNA is transcribed from the *CYP19A* gene, it diffuses to a ribosome to form an mRNA–ribosome complex. The tRNAs bind to AA to form tRNA–AA complexes, which bind to the *CYP19A* mRNA–ribosome complex for translation of *CYP19A* mRNA and subsequent synthesis of the CYP19A protein. In the ovary compartment, the model has zero-order synthesis and first-order degradation of AA, and translation of CYP19A is described by Michaelis–Menten kinetics (Jewett et al., 2009). The time-varying concentrations of substrates are described by dynamic mass balances. We can express the dynamic mass balance for the substrates in the compartment y with volume V_y as:

$$V_y \frac{dC_{x,y}}{dt} = P_{x,y} - U_{x,y} - D_{x,y} + I_{x,y} - S_{x,y} \quad (1)$$

where $C_{x,y}$ is the concentration of substrate x in compartment y, $P_{x,y}$ is the production rate of substrate x in compartment y, $U_{x,y}$ is the utilization rate of substrate x in compartment y, $D_{x,y}$ is the degradation rate of substrate x in compartment y, $I_{x,y}$ is the import rate of substrate x into compartment y, and $S_{x,y}$ is the secretion rate of substrate x from compartment y. The first two terms in the right side of Eq. (1) represent the net metabolic reaction rate of substrate x. The last two terms represent the net uptake or release rate of substrate x in compartment y. The complete set of equations for the model is provided in the Supplementary Data.

2.3. Parameter estimation

The model consists of physiological and biochemical parameters, including tissue compartment volumes, blood flow rates, equilibrium partition coefficients, and biochemical reaction rates (i.e. transcription, translation, metabolism, transport, and degradation). As in the previous model (Breen et al., 2013), the extended model utilizes measured volumes of the major tissue compartments (ovary, liver, brain) and the whole body, and determined physiological parameter values from the literature. Based on experimental results (Villeneuve et al., 2013), the equilibrium tissue:blood partition coefficients for E2, and blood:water and tissue:blood partition coefficients for FAD were assumed to be one. In the extended model, there are 28 biochemical parameters affecting the dose–response and time-course behaviors of *CYP19A* mRNA and E2 in FAD-exposed animals; literature-reported values were used for five parameters as in the previous model, and 23 parameters were estimated using the mean E2 concentrations from the fathead minnow studies. We utilized measured plasma E2 data from the first and second experiments for parameter estimation and ovarian *CYP19A* mRNA data from the first and second experiments, along with plasma E2 data from the third experiment for model validation. The definitions and values of physiological constants and fixed biochemical parameters, and the measured E2 and *CYP19A* mRNA data were previously described in detail by Breen et al. (2013).

The ordinary least squares method was used to estimate the following 23 biochemical parameters from the fathead minnow E2 time-course data (see Table 1): 15 parameters in the ovary compartment ($k_{syn\_mRNA\_basal}$, $k_{syn\_mRNA\_max}$, k_{loss_mRNA}, $V_{max\_syn\_CYP19A}$, $K_{m\_syn\_CYP19A}$, k_{loss_CYP19A}, K_{i_FAD}, $K_{a\_syn\_mRNA}$, k_{rib_on}, k_{rib_off}, k_{syn_AA}, k_{loss_AA}, A_{rib_total}, k_{tRNA_on}, k_{tRNA_off}), two parameters in the liver compartment (k_{loss_FAD}, k_{loss_E2}), four parameters in the brain compartment ($k_{0\_syn\_LHFSH}$, k_{loss_LHFSH}, k_{LHFSH}, K_{i_E2}), and two parameters in the venous blood compartment (k_{LHFSH_off}, k_{loss_LHFSH}). Let n_d be the number of time points in the E2 time-course data for the d^{th} FAD dose (including control); $C^{d,i}_{E2,blood}$ be the measured E2 plasma concentrations for the d^{th} FAD dose at the i^{th} time; $C_{E2,blood}(t_i; C^d_{FAD}, \vec{k})$ be the model-predicted concentrations of E2 in the venous blood compartment at the i^{th} time, t_i, for the d^{th} FAD dose (including control), C^d_{FAD}, with parameter set $\vec{k}$ for $d = 1,2,3,4$, and $i = 1,\ldots n_d$. Then, the least squares estimate k^* is the parameter vector $\vec{k}$ which minimizes the cost function

$$J(\vec{k}) = \sum_{d=1}^{4} \sum_{i=1}^{n_d} \left(C^{d,i}_{E2,blood} - C\left(t_i; C^d_{FAD}, \vec{k}\right)\right)^2. \quad (2)$$

Parameters were estimated with an iterative nonlinear optimization algorithm using MATLAB R2010a (Mathworks, Natick, MA, USA) software. We chose the Nelder–Mead simplex method (MATLAB function: fminsearch) for its relative insensitivity to the initial parameter values as compared to other common methods, such as Newton's method, and its robustness to discontinuities (Nelder and Mead, 1965). We confirmed convergence to a solution after the parameter search terminated.

2.4. Sensitivity analysis

We performed a sensitivity analysis to examine model parameter uncertainty using a previously described method (Breen et al., 2013). The key purpose of sensitivity analysis is to identify the main contributors to the variation in the model outputs by ordering the parameters; parameters with high sensitivity are more important for the model output than parameters with low sensitivity. Briefly, the sensitivity function relates changes of the model output to changes in the model parameters. We calculated the relative sensitivity functions $R_{E2,blood,k_i}(t)$ and $R_{mRNA,ovary,k_i}(t)$ with respect to the parameters k_i for each of the model-predicted concentrations $C_{E2,\ blood}$ and fold changes of *CYP19A* mRNA in the ovary compartment $F_{mRNA,ovary}$, respectively. MATLAB was used to numerically solve the partial derivatives of $R_{E2,blood,k_i}(t)$ and $R_{mRNA,ovary,k_i}(t)$ for control and each FAD dose. To

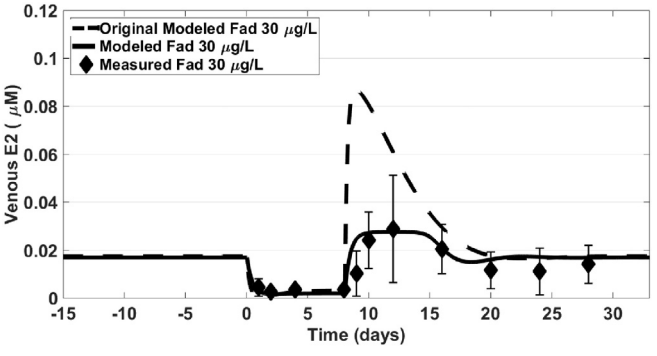

Fig. 3. Comparison of new and original model predictions for FAD 30 μg/L. Model-predictions were plotted as a function of days during pre-exposure (−15–0 days), exposure to FAD (0–8 days), and post-exposure (8–33 days), and compared with measurements (mean ± SD) for plasma E2 concentrations. Model-predictions were compared with measurement data from two experiments: 30 μg/L—four sampling times during exposure and seven sampling times post-exposure.

rank the relative sensitivities, we calculated the L2 norm across time for each relative sensitivity function as described by

$$\left\|R_{\mathrm{E2,blood},k_i}\right\|_{\mathscr{L}^2} = \sqrt{\int \left|R_{\mathrm{E2,blood},k_i}(t)\right|^2 dt} \tag{5}$$

and

$$\left\|R_{\mathrm{mRNA,ovary},k_i}\right\|_{\mathscr{L}^2} = \sqrt{\int \left|R_{\mathrm{mRNA,ovary},k_i}(t)\right|^2 dt}. \tag{6}$$

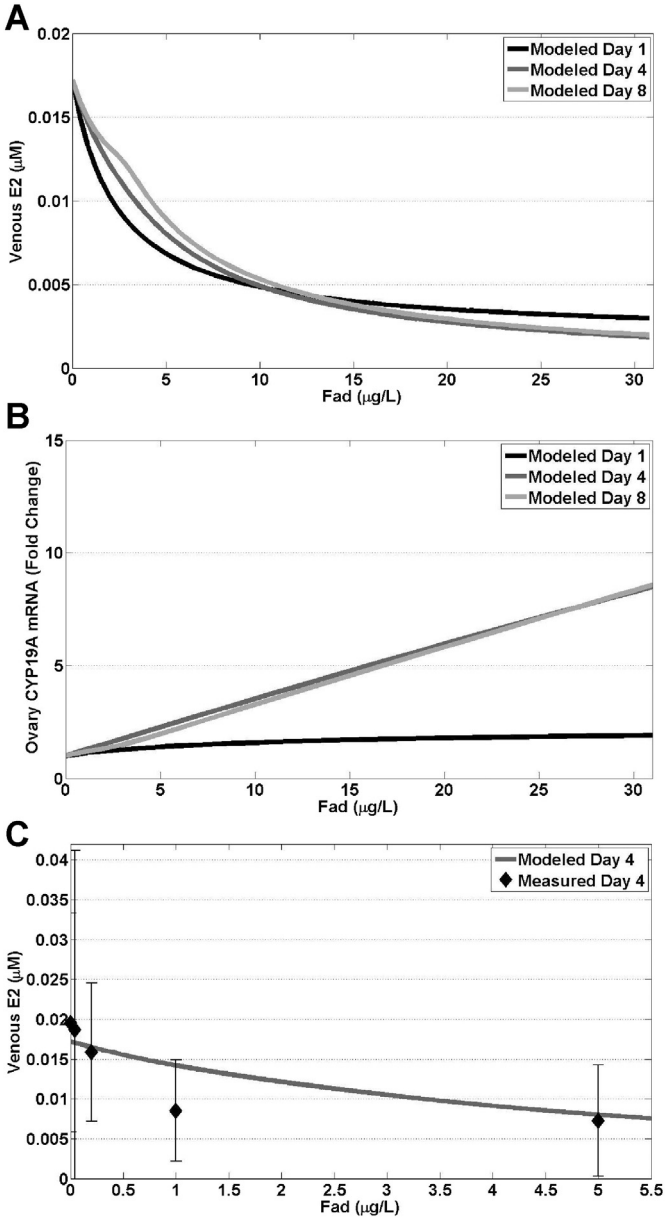

Fig. 4. Modeled dose–response during FAD exposure. Model predictions were plotted as a function of FAD concentrations for venous E2 concentrations (A,C) and ovary CYP19A_mRNA fold changes relative to controls (B) during exposure to FAD on days 1, 4, and 8 (2024, 2096, and 2192 h). For day 4 (C), measured venous E2 concentrations for five FAD concentrations (0, 0.04 0.2, 1, 5 μg/L) with n = 11 or 12 were plotted with model predictions. Same model predictions are shown in A and C for FAD concentrations between 0 and 5.5 μg/L.

3. Results

3.1. Mathematical model of HPG-axis

Table 1 shows the estimated biochemical parameter values determined by fitting the model predictions to the measured mean plasma E2 concentrations for all four FAD doses from the two time-course studies. The time for convergence to the solution for the nonlinear parameter estimation was typically around 4 h on an Intel Core 2 Duo processor using MATLAB.

For plasma E2 concentrations, we compared the model-predicted concentrations with the time-course measurements. Overall, the model-predicted E2 concentrations correspond closely to the mean time-course measurements for all four doses (Fig. 2A–D). For the high FAD dose (30 μg/L), the extended model performed markedly better than the previous model (Fig. 3, Breen et al., 2013), the differences of an overestimate/underestimate from the previous model are reduced by 50, 17, 609, 222, 107, 43, 14, and 3% at 1, 2, 9, 10, 12, 16, 20, and 28 d, respectively. Also, the Euclidean norm of the errors for the extended model, as compared to previous model, was reduced from 0.102 to 0.017 μg/L. The extended model better captured the mean time-course behavior for the 30 μg/L FAD treatment, which was substantially reduced within 1 d of exposure to FAD, remained reduced throughout the exposure period, and rebounded at 2 d post-exposure, before returning to control levels following 8 or more d of recovery in clear water (Fig. 2D). For the other FAD doses, the extended model performed similarly to the original model (Breen et al., 2013). The Euclidean norms of the errors for the extended model were 0.015, 0.015, 0.038, whereas the previous model were 0.015, 0.016, 0.035 for the control, 0.5, and 3 μg/L FAD doses, respectively. In the 3 μg FAD/L treatment, the

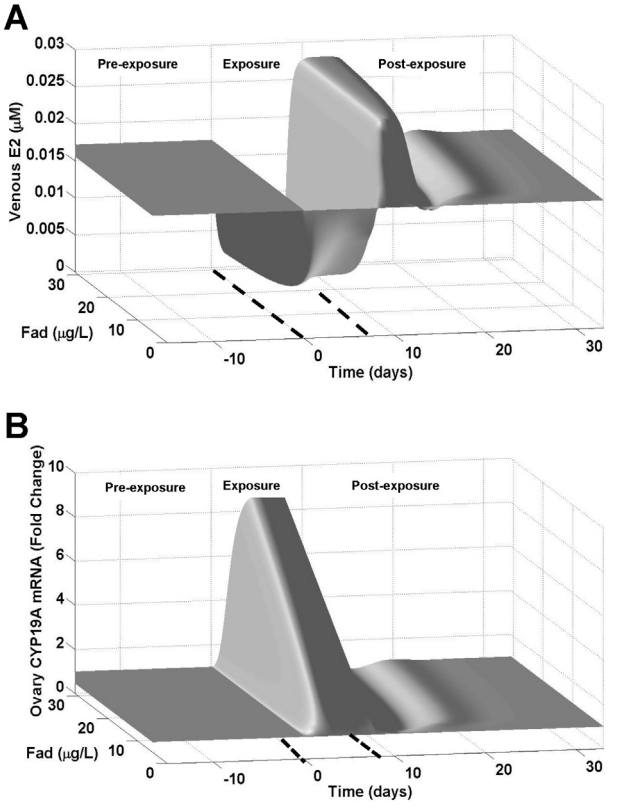

Fig. 5. Model predictions plotted as a function of FAD concentration and time during pre-exposure (−15–0 days), exposure to FAD (0–8 days), and post-exposure (8–33 days) for venous E2 concentrations (A) and ovary CYP19A_mRNA fold changes relative to controls (B).

extended model continued to capture the plasma E2 compensation during exposure, and the overshoot and return to control levels once the FAD exposure was terminated (Fig. 2C).

Fig. 4A shows the model-predicted venous E2 dose–response during FAD exposure on d, 1, 4, and 8. For FAD doses between 0 μg/L and 10 μg/L, the model predictions monotonically decreased across dose, with FAD exposure on d 1 having the lowest venous E2 concentration and d 8 having the highest venous E2 concentration, the same as the original model predicted. The model predictions continued to decrease monotonically across doses for FAD dose greater than 10 μg/L, with E2 concentrations on d 1 decreasing slower than on d 4 and 8. As a result, FAD exposure on d 1 had the highest venous E2 concentration and d 4 and 8 had similar venous E2 concentrations at higher FAD treatments. In contrast, the previous model predictions had the lowest venous E2 concentration on FAD exposure d 1 and the highest venous E2 concentration on FAD exposure d 8 at higher FAD doses. Fig. 5A provides a summary of model predictions for venous E2 concentrations plotted as a function both of FAD concentration and time.

We also compared the model-predicted and measured ovary *CYP19A* mRNA fold changes to validate our extended model. The model-predicted ovary *CYP19A* mRNA fold change corresponds well to the average time-course behavior of the measurements for all four doses (Fig. 2E–H). Fig. 4B shows the model-predicted ovary *CYP19A* mRNA dose–response for FAD exposure on d 1, 4, and 8. The model predictions monotonically increased across dose, with the lowest ovary *CYP19A* mRNA predicted for FAD exposure on d 1: similar to the original model. For d 4 and 8, the model predicted similar ovary *CYP19A* mRNA fold changes as a function of FAD dose, whereas the previous model predicted higher ovary *CYP19A* mRNA fold changes on d 4 than on d 8 (Breen et al., 2013). Fig. 5B provides an integrated summary of the predictions for ovary *CYP19A* mRNA fold changes are plotted both as a function of FAD concentration and time.

Model predictions were compared to plasma E2 concentrations from the 4-d exposure study to further validate our model: this dataset was not used in the model development. Even though all five FAD doses (0, 0.04, 0.2, 1, and 5 μg FAD/L) used for model validation differed

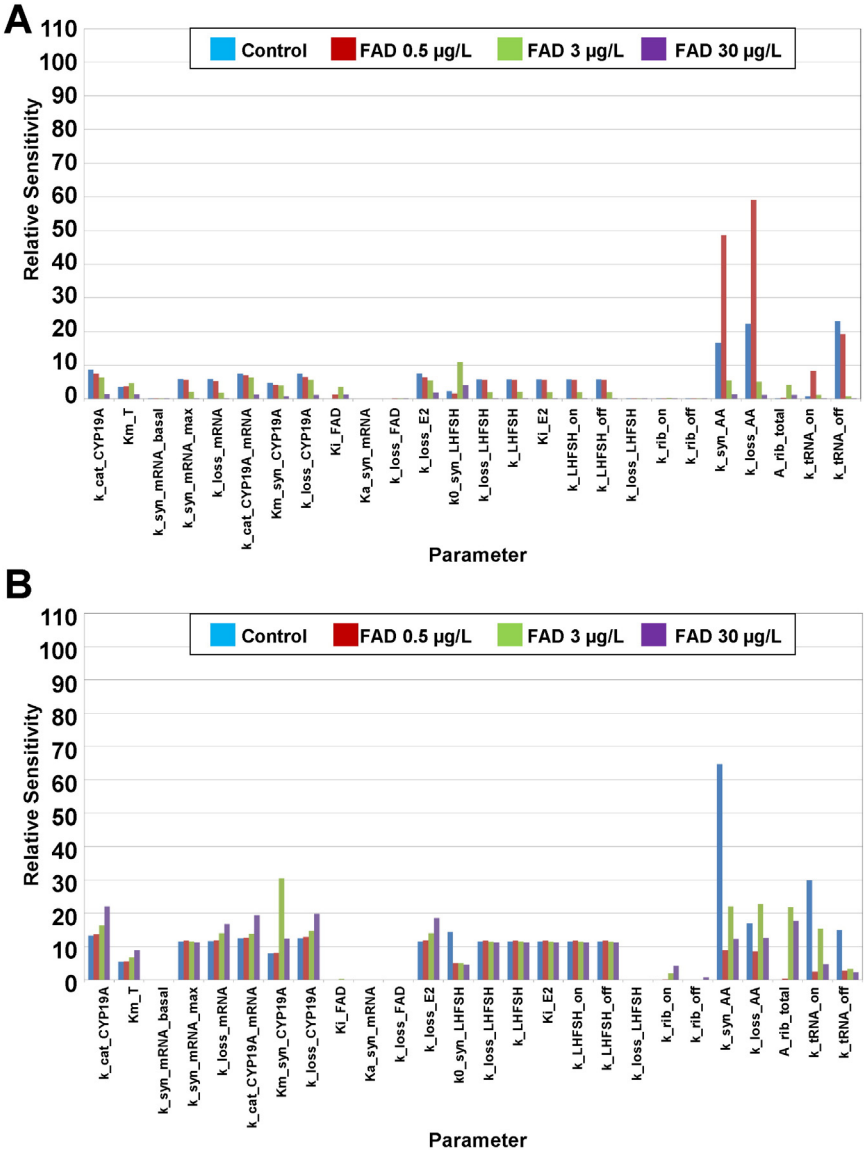

Figure 6

Fig. 6. Relative sensitivities for modeled E2 plotted as a function of the 26 biochemical model parameters for control and three FAD concentrations (0.5, 3, and 30 μg/L). Each bar represents the L^2 norm of the relative sensitivities across time during exposure (0–8 days; A) and post-exposure (8–33 days; B). The values indicate the degree to which changes in parameter values lead to changes in model outputs.

from the FAD doses used for model calibration, the model-predicted dose–response curve for venous E2 corresponds closely to measured plasma E2 (Fig. 4C).

3.2. Sensitivity analysis

The relative sensitivities for modeled E2 and *CYP19A* mRNA, respectively, with respect to each of the 26 biochemical model parameters are shown for the control and three FAD test concentrations (0.5, 3, and 30 μg/L) during exposure and post-exposure (Figs. 6 and 7). Overall, E2 (Fig. 6) and *CYP19A* mRNA (Fig. 7) are highly to moderately sensitive to 17 model parameters during exposure and post-exposure, including 11 parameters associated with CYP19A protein synthesis; six parameters, $k_{syn\_mRNA\_basal}$, $K_{a\_syn\_mRNA}$, k_{loss_FAD}, k_{loss_LHFSH}, k_{rib_on}, k_{rib_off} are insensitive. Of these six parameters, four ($k_{syn\_mRNA\_basal}$, $K_{a\_syn\_mRNA}$, k_{loss_FAD}, k_{loss_LHFSH}) are also not sensitive for E2 and *CYP19A* mRNA in the original model (Breen et al., 2013).

4. Discussion

Breen et al. (2013) developed a mechanistic mathematical model for the HPG axis in female fathead minnows to predict the dose–response, time-course behaviors for endocrine effects of the aromatase inhibitor, FAD. The model included a regulatory feedback loop within the HPG axis that facilitates adaptive responses in plasma E2 concentrations and *CYP19A* mRNA to FAD. The previous model captured the adaptive changes in plasma E2 concentrations occurring during exposure, and the overshoot observed post-exposure for the 3 μg/L FAD dose, along with the up-regulation of ovary *CYP19A* mRNA production occurring during exposure for both the low (3 μg/L) and high (30 μg/L) FAD treatment groups. However, the model did not provide good predictions of plasma E2 concentrations for the high dose (30 μg/L FAD) treatment, which was significantly reduced throughout the exposure period and substantially different from the response at the lower FAD concentrations. These experimental data and modeling results prompted us to refine the model in the current study to examine the hypothesis that

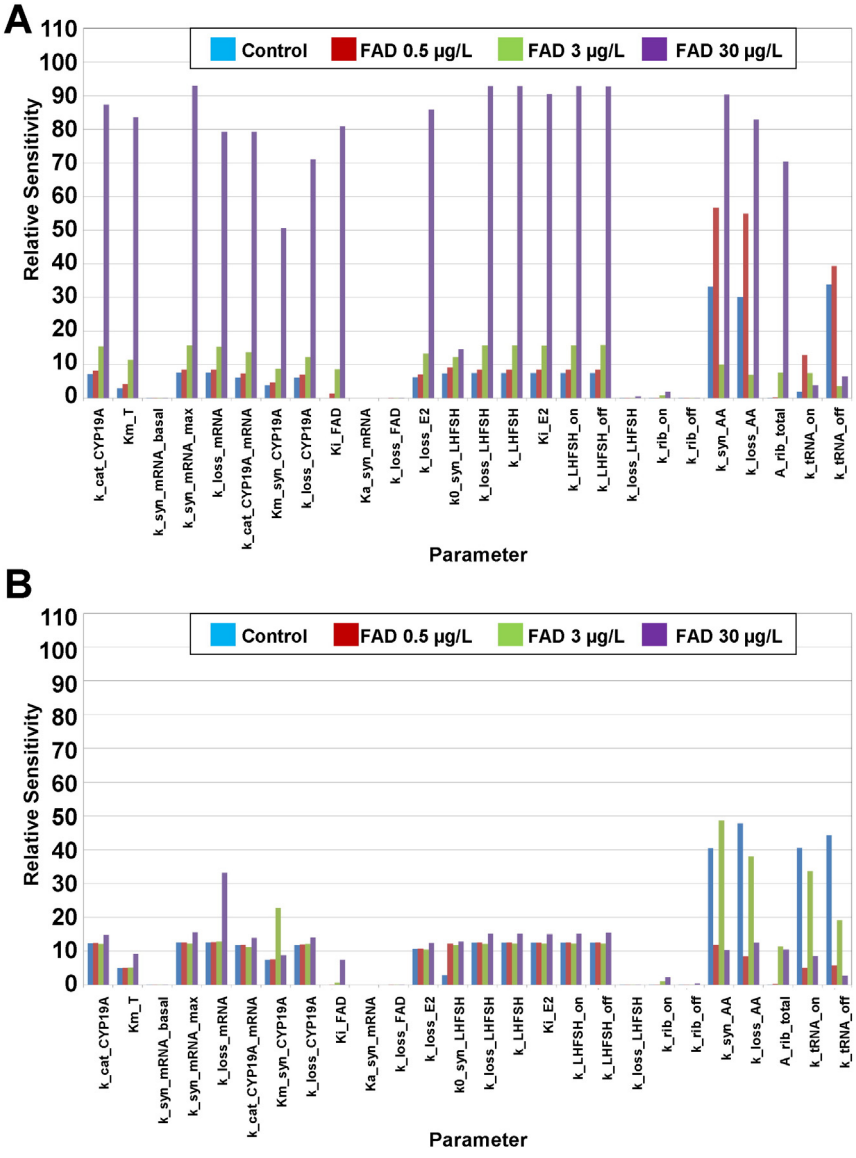

Fig. 7. Relative sensitivities for modeled CYP19A_mRNA plotted as a function of the 26 biochemical model parameters for control and three FAD concentrations (0.5, 3, and 30 μg/L). Each bar represents the L^2 norm of the relative sensitivities across time during exposure (0–8 days; A) and post-exposure (8–33 days; B). The values indicate the degree to which changes in parameter values lead to changes in model outputs.

an additional biological mechanism was needed. Since protein synthesis controls the amount of CYP19A involved in the conversion of T into E2, we investigated protein synthesis as a possible factor influencing compensation. Specifically, we extended the computational model of the HPG axis to include a pathway for protein synthesis to address the main limitation of the previous HPG axis model (Breen et al., 2013). We modeled the pathway for protein synthesis accounting for levels of mRNA, ribosomes, tRNA, and AA, which control the rate of protein synthesis for CYP19A. The extended model was evaluated with measurements of plasma E2 data and ovarian *CYP19A* mRNA for eight FAD test concentrations. The results support our hypothesis. By including a pathway for protein synthesis of CYP19A, the extended model significantly improved the model fit for the dynamic E2 concentrations at high FAD dose (30 μg/L FAD) treatment, while maintaining good model fits of dynamic E2 concentrations for controls and the lower doses (0.5 and 3 μg/L FAD), despite significant differences in data behavior between high and low doses. The extended model was also capable of predicting the dynamic *CYP19A* mRNA fold changes for all four doses during the two time-course studies, and the venous E2 dose–response during a 4-d exposure at 0, 0.04, 0.2, 1, and 5 μg FAD/L. Moreover, our sensitivity analysis indicates that CYP19A protein synthesis plays an important role in the revised model, since both E2 and *CYP19A* mRNA were highly to moderately sensitive to the parameters associated with the protein synthesis.

Our study demonstrates that the detailed modeling of protein synthesis improves the model performance by including limitation for CYP19A protein induction for high FAD concentrations. Since AA, tRNA, and ribosomes will be in excess under normal conditions, as they are needed for synthesis of thousands of proteins in the cells (Bruce et al., 2002; Campbell, 1996), AA supply and the abundance of tRNA and ribosomes may become limiting only at very high protein abundance. One biologically realistic hypothesis for the limitation for CYP19A protein induction is that under stress conditions, such as high FAD concentrations, the total stress proteins rise to an abundance that is substantial compared to the total CYP19A proteins. Stress proteins are a suite of highly conserved proteins, which are produced in the cell under the exposure to stressful environmental conditions, such as chemical exposures, elevated temperatures, ultraviolet lights (Sanders and Martin, 1993; Gupta et al., 2010). One study showed that stress proteins concentrations were elevated, relative to laboratory controls, in mussels and fish tissue when they were exposed to chemicals in the environment (Sanders and Martin, 1993). We hypothesize that under high FAD concentrations, the production of stress proteins are upregulated as part of the stress response, which results in competition of available AA, tRNA, and ribosomes to limit CYP19A protein induction. While our results indicate that the availability of amino acids could be rate-limiting in the production of new CYP19A protein, it should be noted that other steps associated with the regulation of protein synthesis but not explicitly represented in the model, could also be rate-limiting. For example, regulation of transcription of the aromatase gene is multifactorial, and mRNA is processed to remove introns and interacts with miRNA. A future study with collection of stress protein concentrations time course data and inclusion of stress protein pathways in our model could be used to validate our hypothesis.

5. Conclusions

The extended model contributes to ongoing efforts to understand and simulate biological responses to endocrine active chemicals, including aromatase inhibitors. Development of a computational system model that incorporates this additional biological mechanism provides a better understanding of possible adaptive responses, which can refine descriptions of dose–response time-course behaviors that differ substantially from low dose to high dose regimes. The knowledge obtained from iterations in model development, refinement, and empirical testing can help us to better understand the biology underlying toxicological responses to endocrine active chemicals, and can be applied to help reduce the uncertainty of dose–response assessments in support of quantitative risk assessments, a need identified as critical to supporting new approaches to regulatory toxicology (National Research Council, 2007).

Acknowledgements

We thank Qiang Zhang, Sudin Bhattacharya, and Wan-Yun Cheng for their review comments and helpful suggestions. Although this manuscript was reviewed by the U.S. Environmental Protection Agency and approved for publication, it may not reflect official Agency policy. Mention of trade names or commercial products does not constitute endorsement or recommendation for use.

Appendix A. Supplementary data

Supplementary data to this article can be found online at http://dx.doi.org/10.1016/j.cbpc.2016.02.002.

References

Ankley, G.T., Bencic, D.C., Breen, M.S., Collette, T.W., Conolly, R.B., Denslow, N.D., Edwards, S.W., Ekman, D.R., Garcia-Reyero, N., Jensen, K.M., Lazorchak, J.M., Martinović, D., Miller, D.H., Perkins, E.J., Orlando, E.F., Villeneuve, D.L., Wang, R.L., Watanabe, K.H., 2009. Endocrine disrupting chemicals in fish: developing exposure indicators and predictive models of effects based on mechanism of action. Aquat. Toxicol. 92, 168–178.

Breen, M., Villeneuve, D.L., Ankley, G.T., Bencic, D.C., Breen, M.S., Watanabe, K.H., Lloyd, A.L., Conoll, R.B., 2013. Developing predictive approaches to characterize adaptive responses of the reproductive endocrine axis to aromatase inhibition: II. Comput. Model. Toxicol. Sci. 133, 234–247.

Bruce, A., Johnson, A., Lewis, J., Raff, M., Roberts, K., Walter, P., 2002. Molecular Biology of the Cell. fourth ed. Garland Science, New York, NY.

Campbell, N.A., 1996. Biology. fourth ed. The Benjamin/Cummings Publishing Company, San Francisco, CA.

Cooper, R.L., Kavlock, R.J., 1997. Endocrine disruptors and reproductive development: a weight-of-evidence overview. J. Endocrinol. 152, 159–166.

Daston, G.P., Cook, J.C., Kavlock, R.J., 2003. Uncertainties for endocrine disrupters: our view on progress. Toxicol. Sci. 74, 245–252.

Drenth, H.J., Bouwman, C.A., Seinen, W., Van den Berg, M.V., 1998. Effects of some persistent halogenated environmental contaminants on aromatase (CYP19) activity in the human choriocarcinoma cell line JEG-3. Toxicol. Appl. Pharmacol. 148, 50–55.

Food Quality Protection Act, 1996. Public Law 104–170.

Gupta, S.C., Sharma, A., Mishra, M., Mishra, R.K., Chowdhuri, D.K., 2010. Heat shock proteins in toxicology: how close and how far? Life Sci. 86, 377–384.

Hutchinson, T.H., Ankley, G.T., Segner, H., Tyler, C.R., 2006. Screening and testing for endocrine disruption in fish-biomarkers as "signposts," not "traffic lights," in risk assessment. Environ. Health Perspect. 114, 106–114.

Jewett, M.C., Miller, M.L., Chen, Y., Swatz, J.R., 2009. Continued protein synthesis at low [ATP] and [GTP] enables cell adaptation during energy limitation. J. Bateriology 191, 1083–1091.

Miller, W., 1988. Molecular biology of steroid hormone synthesis. Endocr. Rev. 9, 295–318.

National Research Council, 2007. Toxicity Testing in the 21st Century: A Vision and a Strategy. National Academy Press, Washington, DC.

Nelder, J.A., Mead, R., 1965. A simplex method for function minimization. Comput. J. 7, 308–313.

Petkov, P.I., Temelkov, S., Villeneuve, D.L., Ankley, G.T., Mekenyan, O.G., 2009. Mechanism-based categorization of aromatase inhibitors: a potential discovery and screening tool. SAR QSAR Environ. Res. 20, 657–678.

Ralston-Hooper, K.J., Turner, M.E., Soderblom, E.J., Villeneuve, D.L., Ankley, G.T., Moseley, M.A., Hoke, R.A., Ferguson, P.L., 2013. Application of a label-free, gel-free quantitative proteomics method for ecotoxicological studies of small fish species. Environ. Sci. Technol. 47, 1091–1100.

Safe Drinking Water Act Amendments, 1996. Public Law 104–182.

Sanders, B.M., Martin, L.S., 1993. Stress proteins as biomarkers of contaminant exposure in archived environmental samples. Sci. Total Environ. 139/140, 459–470.

Sanderson, J.T., 2006. The steroid hormone biosynthesis pathway as a target for endocrine-disrupting chemicals. Toxicol. Sci. 94, 3–21.

U.S. Environmental Protection Agency, 1998. Endocrine Disruptor Screening Program. Fed. Regist. 63 (154), 42852–42855 (August 11).

U.S. Environmental Protection Agency, 2009. Endocrine Disruptor Screening Program (EDSP): announcing the availability of the Tier 1 screening battery and related test guidelines. Fed. Regist. 74 (202), 54415–54422 (October 21).

Villeneuve, D.L., Breen, M., Bencic, D.C., Cavallin, J.E., Jensen, K.M., Makynen, E.A., Thomas, L.M., Wehmas, L.C., Conoll, R.B., Ankley, G.T., 2013. Developing predictive approaches to characterize adaptive responses of the reproductive endocrine axis to aromatase inhibition: I. Data Generation in a Small Fish Model. Toxicol. Sci. 133, 225–233.

Villeneuve, D.L., Mueller, N.D., Martinovic, D., Makynen, E.A., Kahl, M.D., Jensen, K.M., Durhan, E.J., Cavallin, J.E., Bencic, D., Ankley, G.T., 2009. Direct effects, compensation, and recovery in female fathead minnows exposed to a model aromatase inhibitor. Environ. Health Perspect. 117, 624–631.

Vinggaard, A.M., Hnida, C., Breinholt, V., Larsen, J.C., 2000. Screening of selected pesticides for inhibition of CYP19 aromatase activity *in vitro*. Toxicol. in Vitro 14, 227–234.

Zacharewski, T., 1998. Identification and assessment of endocrine disruptors: limitations of in vivo and in vitro assays. Environ. Health Perspect. 106, 577–582.